Lifetime of a hydrogen atom in an intense radiation field

Niels R. Walet*
FOM–Institute for Atomic and Molecular Physics, Kruislaan 407, 1098 SJ Amsterdam, The Netherlands
(Received 26 August 1988; revised manuscript received 29 September 1989)

The lifetime of an atom in a high-frequency high-intensity laser field is studied. A coupled-channel formalism is developed, based on a well-known high-frequency theory, that describes the behavior of an atom in a laser field. Numerical results are obtained using a finite-difference approximation in combination with a two-center complex scaling technique. The complex scaling method is also shown to be very well suited for calculations on diatomic molecules. Several numerical results are used to illustrate the qualitative features of the method. We show that our theory is formally (though not in practice) equal to other methods that have been used heretofore. It will be shown that, for high-frequency and high-intensity laser fields, the present method can be used to calculate resonance energies using only a few channels.

I. INTRODUCTION

The effects of lasers on atoms have become very complicated with the advent of lasers that are strong enough to compete with the static attraction an electron "feels" in the first Bohr orbit of hydrogen. (For a linearly polarized laser this corresponds to an intensity $I_0=3.5\times10^{16}$ W/cm^2.) For these intensities one can no longer consider the effect of single photons separately, as can, for instance, be seen from the phenomenon of excess photon ionization, where outcoming electrons pick up several times the photon energy in excess of the minimum number needed to ionize.[1]

In the (idealized) case where the duration of the laser pulse is long compared to the inverse frequency, so that one has a large number of oscillations in such a pulse, it might be justified to approximate the pulse by a plane or standing wave. Since the size of a laser focus is usually of macroscopic dimension, the spatial extension of the fields can be disregarded when considering its effects on an individual atom. If, furthermore, the velocity of a free electron in the laser field is low compared to the speed of light, the nonrelativistic Schrödinger equation is applicable. As usual, the nucleus is considered as an infinitely heavy point charge that exerts a Coulomb attraction on the electron(s). The approximations in the treatment of the laser field made here are common to most theoretical studies of multiphoton effects, although some work has been performed on multiphoton effects in noisy lasers[2] and Kulander[3] has studied the effect of the temporal profile of the laser pulse using the time-dependent Hartree-Fock equation.

For intensities that are much smaller than 10^{16} W/cm^2 one can calculate the effects of the laser through perturbation theory in the intensity of the laser (for reviews see the papers in Ref. 4). For stronger lasers perturbation theory is no longer good enough and one needs to consider other means. Two methods have been employed: the Floquet supermatrix method by Chu, and co-workers[5,6] and the integral-equation approach by Tang and Shakeshaft.[7,8] In essence, both these methods take the unperturbed atom as a reference system and perform a kind of coupled-channel calculation based on this reference problem. These methods can be applied when we do not consider too strong a distortion of the hydrogen atom; in fact, these methods are quite successful for intensities up to I_0. If we go to much higher intensities these methods become highly impractical, however. This is reflected in the fact that one will not be able to obtain convergent results with a reasonable number of channels.

For this reason a completely different starting point has been taken for large intensities and high frequencies. If one considers an atom that is subject to a radiation field for all times, it appears useful to include part of the interaction of the electron with the laser field in the reference problem. This can be accomplished through the choice of an accelerated coordinate frame, where the inertial forces compensate the $\mathbf{p}\cdot\mathbf{A}$ term in the Hamiltonian.[9] This idea has been applied several times in the theory of multiphoton processes; see Refs. 10–14.

The new Schrödinger equation contains a new reference system: if we take both the intensity and frequency to ∞, keeping the ratio $\sqrt{I}/\omega^2$ fixed we obtain a radiation dressed bound-state problem. The resulting Schrödinger equation has been studied exhaustively in Ref. 15. The purpose of the present paper is to go beyond this static problem and to study the use of a coupled-channel approach based on this new reference system. This should be most fruitful for high frequencies (the meaning of the world high will be specified later).

Bardsley and Comella[16] have recently studied such an approach numerically for a simple one-dimensional potential, where one can easily obtain the quasienergies by integrating the time-dependent Schrödinger equation. As expected their results show that, in the large ω limit, the quasienergies are very close to the bound-state energies of the corresponding reference problem. The coupled-channel problem we are studying here provides a means to study the same behavior for the three-dimensional Coulomb potential.

The paper is organized as follows. We start by discussing some theoretical background. In Sec. II we give a

derivation of the Schrödinger equation in the accelerated frame. We discuss some ideas about spectra and the calculations of resonances (an atom in an intense laser field is not stable, so all bound states become resonances). In Sec. III the structure of the potentials appearing in the modified Schrödinger equation will be studied in more detail. This leads to a natural extension of the usual spectral deformation as obtained through the complex scaling transform. In Sec. IV a modified form of the variation functional, appropriate for complex symmetric Hamiltonians, will be introduced. The numerical approach to solution of the coupled-channel equations is discussed in Sec. V and the Appendix. We end the description of the formalism in Sec. VI with a discussion of the relation of results obtained by approximate solution of the Schrödinger equation in the accelerated frame to results obtained in the lab frame.

The method developed in the previous sections is subsequently applied to a few examples (Sec. VII). We first check the qualitative features of the theory (Sec. VII A), in cases where we are not interested in high-accuracy calculations. For these calculations we do not make use of the sparse matrix structure of the problem, but we calculate all eigenvalues to illustrate the qualitative features of the method. We comment on some of the differences in behavior compared with the usual basis set methods.

Then (Sec. VII B) we report some accurate calculations, using the sparse matrix structure. We show that the method can be used to obtain results close to those already reported in the literature for relatively weak fields, but that its main power lies in the region where α_0 is greater than 1. As an example, we study the frequency dependence of the lifetime and energy of the ground state for fixed α_0. This shows where the bound-state problem used as a starting point is a good approximation.

Finally, in Sec. VIII, a few conclusions are drawn and an outlook is given.

It should be noted here that atomic units ($\hbar=e=m_e=1$, $\epsilon_0=1/4\pi$) are used throughout this paper.

II. HAMILTONIANS AND SPECTRA

Consider an atom in a linearly polarized classical radiation field. This can be described by a time-dependent Schrödinger equation in the minimal coupling scheme, where retardation is disregarded and the field is approximated by a standing wave

$$\{\tfrac{1}{2}[\mathbf{p}-\mathbf{A}(t)]^2+V(\mathbf{r})\}\phi(\mathbf{r},t)=-i\partial_t\phi(\mathbf{r},t)\ , \tag{1}$$

$$\mathbf{A}(t)=\mathbf{e}a\cos(\omega t)\ . \tag{2}$$

It is useful to perform a combination of transformations on ϕ,

$$\phi=V(U(\chi))\ , \tag{3}$$

with

$$(Uf)(\mathbf{r},t)=\exp\left[-\frac{i}{2}\int^t A^2(t')dt'\right]f(\mathbf{r},t)\ , \tag{4}$$

and

$$\begin{aligned}&(Vf)(\mathbf{r})=f(\mathbf{r}+\boldsymbol{\alpha}(t))\ ,\\ &\boldsymbol{\alpha}(t)=\mathbf{e}\alpha_0\sin(\omega t)\ ,\end{aligned} \tag{5}$$

[with $\alpha_0=a/\omega=(I/I_0)^{1/2}\omega^2$ and $I_0=3.5\times10^{16}$ W/cm^2].

The transformation V was first introduced by Kramers[9] in a different context and first applied to multiphoton processes by Henneberger.[10] It is a change-of-coordinate transformation where the new coordinates are chosen in such a way that the origin follows the quiver motion, the orbit of a free electron in the laser field. The Schrödinger equation Eq. (1) is transformed into

$$[\tfrac{1}{2}\mathbf{p}^2+V(\mathbf{r}-\boldsymbol{\alpha}(t))]\chi(\mathbf{r},t)=-i\partial_t\chi(\mathbf{r},t)\ . \tag{6}$$

This equation is, just as Eq. (1), a Schrödinger equation with periodic coefficients. A general statement about such equations is the Floquet theorem [named after Floquet, a pioneer in the field of (ordinary) differential equations with periodic coefficients[17]]. This is a generalization of the well-known transition from the time-dependent to the time-independent Schrödinger equation (see especially Refs. 18 and 19). It is most readily formulated on an extended Hilbert space of quadratic integrable functions in four-dimensional space-time $(\mathbf{r},x_0)$ that are *periodic* in x_0. The Floquet theorem states that in the enlarged Hilbert space we can write a spectral equation, similar to the usual time-independent Schrödinger equation

$$[\tfrac{1}{2}\mathbf{p}^2+p_0+V(\mathbf{r}-\boldsymbol{\alpha}(x_0))]\psi(\mathbf{r},x_0)=E\psi(\mathbf{r},x_0)\ . \tag{7}$$

The energy parameter E is called a quasienergy since it appears as the energy in the usual spectral form of the Schrödinger equation, but describes only part of the time evolution of the wave function,

$$\chi(\mathbf{r},t)=\exp(-iEt)\psi(\mathbf{r},t)\ , \tag{8}$$

where ψ is periodic in t.

We now represent the periodic functions by their Fourier series. If one defines

$$\begin{aligned}&\psi(\mathbf{r},t)=\sum_{n=-\infty}^{\infty}e^{-in\omega t}\psi_n(\mathbf{r})\ ,\\ &V(\mathbf{r},t)=\sum_{n=-\infty}^{\infty}e^{-in\omega t}V_n(\mathbf{r},\alpha_0)\ ,\end{aligned} \tag{9}$$

one obtains the more conventional set of equations

$$\sum_k[(\tfrac{1}{2}\mathbf{p}^2-k\omega)\delta_{kl}+V_{l-k}(\mathbf{r},\alpha_0)]\psi_k=E\psi_l\ . \tag{10}$$

These equations have been studied previously by Gersten and Mittleman[12] and also by Gavrila and Kaminski.[13,14] Note that the operators on the left-hand side of Eq. (10) commute with L_z, so that all values of the magnetic quantum number m can be treated separately. The molecular notation ($\sigma,\pi,\delta,\ldots$ for $|m|=0,1,2,\ldots$) is used for all these symmetry channels. We shall restrict the study in the present paper to the states of σ symmetry, the manifold that includes the ground state.

In practice one will, of course, not consider the infinite problem, Eq. (10), but a limited subset

$$\sum_{m=N_1}^{N_2} [(\tfrac{1}{2}\mathbf{p}^2 - m\omega)\delta_{nm} + V_{n-m}(\mathbf{r},\alpha_0)]\psi_m = E\psi_n \ . \quad (11)$$

This set is a good approximation to the full problem once the number of channels $(N_2 - N_1 + 1)$ is sufficiently high for the value of ω chosen.

In the work of Gavrila and Kaminski the limit $\omega \to \infty$ has been studied in some detail. They have shown that in this limit only a single time-independent equation, corresponding to fixing $k = l = 0$ in Eq. (10), remains. For large but finite frequency the correction to the equations are of order $1/\omega$. The arguments presented by these authors cannot be used to prove convergence of the expansion in $1/\omega$, however, and presumably the series is asymptotic.

The single equation left in the limit $\omega \to \infty$, from now on called the zeroth-order equation,

$$[\tfrac{1}{2}\mathbf{p}^2 + V_0(\mathbf{r},\alpha_0)]\psi_0 = E\psi_0 \ , \quad (12)$$

has an infinite number of bound states ($E < 0$) as well as a continuum for $E > 0$. The zeroth order is a good (asymptotic) approximation as soon as

$$\omega \gg |E_0^m(\alpha_0)| \ , \quad (13)$$

i.e., the frequency must be much larger than the binding energy of the lowest state of the same m quantum number in the field. The eigenfunctions and eigenenergies of this equation have been studied Refs. 10, 12, and 20, but especially in the work of Pont *et al.*[15] The most important results obtained in these last papers are the breakup of the wave function into two parts as α_0 grows, and a simultaneous strong decrease of the ionization potential.

In order to understand the high-frequency condition (13) in the context of frequency and intensity instead of frequency and α_0, the reader is invited to study Fig. 1. There we have plotted the curves $\omega = E(\alpha_0)$ and $1.5E(\alpha_0)$ for the ground state $(1s)$ σ_g. The region where ω is smaller than the energy falls under the curve. As can clearly be seen the high-frequency condition is most readily satisfied for small intensities when the frequency is either very small (e.g., microwave radiation) or very large [vacuum ultraviolet (vuv), x-ray, etc.].

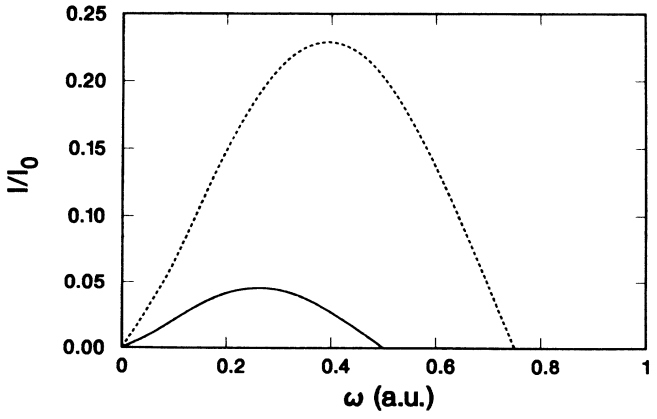

FIG. 1. Functions $\omega = E_0(\alpha_0)$ (solid line) and $\omega = 1.5E_0(\alpha_0)$ (dashed line). In the regions under these curves ω is smaller than 1 (respectively 1.5) times $E(\alpha_0)$.

Let us now return to the coupled-channel problem. If we neglect the "off-diagonal potentials" $(V_i, i \neq 0)$, the spectrum of Eq. (10) is purely continuous from $-\infty$ to ∞, consisting of an infinite multiplet of continua with thresholds at $m\omega$. When the off-diagonal potentials are nonzero but not too strong we expect the same behavior to persist. Since Eq. (10) is invariant under a shift in $\omega, E = E + \omega$, it is clear that the spectrum is periodic with period ω.

Since every channel has open channels (channels it can decay to) under it, one knows that every bound state of Eq. (12) becomes a resonance for finite ω. This situation is depicted in Fig. 2(a), where the first Riemann sheet of the resolvent is plotted. For those readers who are not familiar with this representation, one can equivalently consider this to be the complex energy plane for the S matrix. Bound states show up as poles of the S matrix on the real axis. The continuous spectrum causes a branch cut in the complex plane. Scattering resonances do not lie in the first (physical) Riemann sheet and can only be reached by going into the second Riemann sheet from above the real axis, crossing the branch cut.

The complex scaling method has been applied quite successfully in the problem of calculating resonances (see Refs. 21 and 22 for a practical discussion of the method and Simon[23] for a discussion of the mathematical context). If the potential decays fast enough as $r \to \infty$, it can be shown that the transformation

$$r \to r \exp(-i\theta) \quad (14)$$

in the Hamiltonian results in an operator that has the

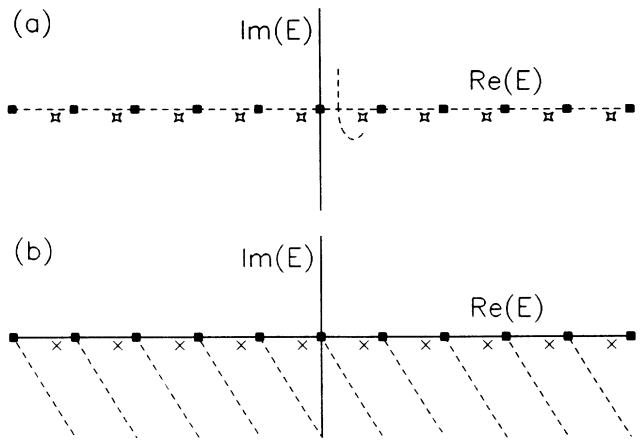

FIG. 2. (a) Continuous spectrum of the complete coupled-channel problem Eq. (10). In order to be able to distinguish the continua, each threshold is indicated by a dot. The stars indicate the position of a resonance. (b) The effect of a complex coordinate transformation on the spectrum sketched in (a). The continua are rotated and the resonances become eigenvalues of the new operator.

same bound states as the original problem, but, depending on the parameter θ, has a complex eigenvalue at the position of a resonance in the S matrix. The Hamiltonian has now become a non-Hermitian operator, and has thus different left and right eigenvectors. If one takes θ purely imaginary, one sees more clearly what this method does, because in that case one ends up with a Hamiltonian with identically the same spectrum as before the transformation, due to the fact that Eq. (14) is just a similarity transformation.

In fact, we can define a unitary transformation U_θ corresponding to Eq. (14),

$$U_\theta f(\mathbf{r}) = e^{-i3\theta/2} f(\mathbf{r}e^{i\theta}) \ . \tag{15}$$

The power of this transformation lies in the fact that, in general, the operator U_θ does not map the Hilbert space of square integrable functions onto itself. Let us, for example, consider a state with complex energy E. In the large r region, where we can neglect the potential, we have

$$\phi \propto \exp(-i\sqrt{E}\, r) \ , \tag{16}$$

which if E has negative imaginary part will grow exponentially, and is not square integrable. If we replace r by $r\exp(i\theta)$, we can see that if $\theta < \arg E$ the function ϕ becomes exponentially damped, and thus can belong to a new space of square integrable wave functions. There is obviously a great similarity with the use of Siegert boundary conditions,[24] where one imposes exponential growth on the wave function. The main advantage of complex scaling is that it reduces calculating resonances to an eigenvalue problem.

Clearly the class of transformations with properties given above is larger than just the single representative. The choice given above is convenient for many problems, and in general allows one to move the continua as depicted in Fig. 2(b). In this way one can construct a new Hamiltonian that is no longer self-adjoint and has complex eigenvalues at the resonance positions. For the problem at hand it is not the right transformation, however, since the potentials are too singular; we shall discuss an appropriate similarity transformation after a study of the structure of the potentials V_n.

III. POTENTIALS V_n AND COMPLEX SCALING

A few simple integrations show that for the hydrogen atom, where $V(\mathbf{r}) = -1/r$, one has

$$V_n(\mathbf{r},\alpha_0) = -\frac{1}{2\pi}\int_{-\pi}^{\pi} \frac{\cos(n\beta)}{|\mathbf{r}-\alpha_0 \mathbf{e}\cos\beta|}\, d\beta \ . \tag{17}$$

The potential V_0 can also be evaluated as a complete elliptic integral

$$V_0 = -\frac{1}{\pi}\frac{1}{(r_+ r_-)^{1/2}} K([(1-\mathbf{r}_+\cdot\hat{\mathbf{r}}_-)/2]^{1/2}) \ , \tag{18}$$

with

$$\mathbf{r}_\pm = \mathbf{r} \pm \alpha_0 \mathbf{e} \ . \tag{19}$$

There is a more natural coordinate frame for the study of these potentials than the Cartesian one. As in the H_2^+ problem these are the prolate spheroidal (also called confocal elliptical) coordinates,[25]

$$\begin{aligned} \xi &= \frac{r_+ + r_-}{2\alpha_0} \in [1,\infty) \ , \\ \eta &= \frac{r_+ - r_-}{2\alpha_0} \in [-1,1] \ , \\ \phi &= \arctan(x/y) \ . \end{aligned} \tag{20}$$

In these coordinates one has

$$\begin{aligned} p^2 &= \frac{1}{\alpha_0^2}\frac{1}{(\xi^2-1)+(1-\eta^2)}[\partial_\xi(\xi^2-1)\partial_\xi + \partial_\eta(1-\eta^2)\partial_\eta] \ , \\ d^3r &= \alpha_0^3[(\xi^2-1)+(1-\eta^2)]d\xi\, d\eta\, d\phi \ , \\ V_n &= -\frac{1}{\pi\alpha_0}\int_{-\pi}^{\pi} \frac{\cos(n\beta)}{[(\xi^2-1)(1-\eta^2)+(\xi\eta-\cos\beta)^2]^{1/2}} d\beta \ . \end{aligned} \tag{21}$$

As one can easily see, the potentials V_n are only singular for $\xi = 1$. Since as $r = (x^2+y^2+z^2)^{1/2}$ grows large one has

$$\xi \to r/\alpha_0, \quad \eta \to \cos\theta \ , \tag{22}$$

it is an obvious alternative to exterior scaling to take ξ to complex values. A very straightforward choice (one should note that the lower boundary $\xi = 1$ remains untransformed, in order to avoid stock terms on partial integration) is

$$\xi^2 - 1 \to e^{-2i\theta}(\xi^2-1) \ . \tag{23}$$

There is a close relation to ordinary complex scaling. We shall not discuss the mathematical details,[26] but will check numerically that the transformation behaves as is expected, i.e., that the continuous spectrum descends under an angle 2θ into the complex plane. The complex scaling transformation U_θ has a somewhat more complicated form than in the radial case:

$$\begin{aligned} U_\theta f(\xi,\eta,\phi) = f([(\xi^2-1)e^{-2i\theta}+1]^{1/2},\eta,\phi) \\ \times \left[\frac{(\xi^2-1)e^{-2i\theta}+(1-\eta^2)}{(\xi^2-1)+(1-\eta^2)}\right]^{1/2} \\ \times \frac{\xi^{1/2}e^{-i\theta}}{[(\xi^2-1)e^{-2i\theta}+1]^{1/2}} \ . \end{aligned} \tag{24}$$

IV. VARIATIONAL FORMULATION OF COMPLEX SCALING

In this section we investigate the variational formulation of the Schrödinger equation after complex scaling. As is well known, the usual time-independent Schrödinger equation is equivalent to the variational principle

$$\frac{\delta I(\phi,\phi')}{\delta\phi} = 0, \quad \frac{\delta I(\phi,\phi')}{\delta\phi'} = 0 \ , \tag{25}$$

with

$$I(\phi,\phi')=(\phi',(H-E)\phi)=\int d^3r\,\overline{\phi'(r)}(H-E)\phi(r)\ . \tag{26}$$

Due to the Hermitian character of H, it does not make a difference whether H acts to the left or right, so that we can take $\phi=\phi'$ and ϕ real, in which case one has

$$\frac{\delta I(\phi,\phi)}{\delta\phi}=0\ . \tag{27}$$

For a complex scaled Hamiltonian one has (U_θ again denotes the transformation that takes the coordinates to complex values)

$$H_\theta=U_\theta^{-1}HU_\theta\ . \tag{28}$$

The "bivariational" equation reads[27]

$$\frac{\delta}{\delta\bar{\phi}'}\ \text{ or }\ \frac{\delta}{\delta\phi}(\phi',(U_\theta^\dagger HU_\theta-E)\phi)=0\ . \tag{29}$$

Of course, one cannot restrict ϕ to be real, but a simple calculation using some properties of inner products and Hermitian conjugation shows that the two resulting equations are

$$\begin{aligned}&(H_\theta-E)\phi=0\ ,\\ &(H_\theta^\dagger-\bar{E})\bar{\phi}'=[\phi'(H_\theta-E)]^\dagger=0\ .\end{aligned} \tag{30}$$

Taking $\phi'=\phi$ thus leads to a consistent variational principle

$$\frac{\delta I_\theta(\phi,\bar{\phi})}{\delta\phi}=0\ , \tag{31}$$

where ϕ is now a complex function.

V. FINITE-DIFFERENCE DISCRETIZATION

Since there is no simple natural set of basis function associated with the zeroth-order Hamiltonian Eq. (12), we prefer to use a purely numerical method. This is different from the Gaussian basis functions employed in Ref. 15. We base the method on the variational equation (31). The form of the integral appearing in this equation

$$I_\theta(\phi)=\int\phi(H_\theta-E)\phi\,d^3r \tag{32}$$

can be simplified by redistributing the action of the kinetic energy operator $-\frac{1}{2}\Delta_\theta$ both to the left and the right by partial integration such that only first derivatives are left. The resulting integrals can be approximated on a grid, using either the finite-difference or finite-element methods (for a representative selection of papers where these methods are applied in quantum physics see Refs. 28–31).

In the present paper we consider only the lowest-order finite-difference approximation, which has the advantage of having an error estimate that contains only low-order derivatives of the wave function. Due to the singular nature of the potential we know that the high-order derivatives on the "line of charges" (the line from $-\alpha_0$ to α_0) are also singular, so that one cannot increase the order of the method without further analysis of the behavior near the singularity.

One further change of coordinate transformation is performed

$$\begin{aligned}&\xi=\cosh\mu\ ,\\ &\eta=\cos\nu\ .\end{aligned} \tag{33}$$

This is most appropriate for H_2^+ since it removes the cusp in the wave function at a Coulomb singularity,[28,29] but since a linear increase in μ means exponential increase in ξ for large radii, it is also useful in the present calculation, where the states also show exponential decrease. For the complex scaled version of the photoionization problem the variational functional obtained through lowest-order finite differences is (for $m=0$, the only symmetry considered in this paper)

$$I(\phi)=\frac{1}{2\alpha_0^2}\left[\frac{1}{h_\mu^2}\sum_{m=0}^{N_\mu-2}\sum_{n=0}^{N_\nu-1}W^1_{m+1/2,n}(\phi_{mn}-\phi_{m+1,n})(V^1_{mn}\phi_{mn}-V^1_{m+1,n}\phi_{m+1,n})\right.$$
$$\left.+\frac{1}{h_\nu^2}\sum_{m=0}^{N_\mu-1}\sum_{n=0}^{N_\nu-2}W^2_{m,n+1/2}(\phi_{mn}-\phi_{m,n+1})(V^2_{mn}\phi_{mn}-V^2_{m,n+1}\phi_{m,n+1})\right]+\sum_{m=0}^{N_\mu-1}\sum_{n=0}^{N_\nu-1}[(V_{mn}-E)g_{mn}\phi^2_{mn}]\ . \tag{34}$$

Here $h_\mu=C_\mu/N_\mu$, $h_\nu=\pi/N_\nu$, where C_μ is some cutoff on the μ coordinate. An index m denotes evaluation at $\mu=(m+\frac{1}{2})h_\mu$ and n evaluation at $\nu=(n+\frac{1}{2})h_\nu$. The explicit form of the functions W^1, W^2, V^1, V^2, and g is given in the Appendix, where Eq. (34) is also derived.

Using Eq. (34), Eq. (31) can be rewritten as (we have abbreviated the two indices m and n by one combined index denoted by i or j)

$$\frac{\partial}{\partial\phi_i}\sum_{j,k}\phi_k(H_{kl}-Eg_l\delta_{kl})\phi_l=0\ , \tag{35}$$

leading to the ordinary eigenvalue equation

$$\sum_j H'_{ij}\phi'_j=E\phi'_i\ , \tag{36}$$

with

$$H'_{ij}=g_i^{-1/2}H_{ij}g_j^{-1/2},\quad \phi'_i=g_i^{1/2}\phi_i\ , \tag{37}$$

where $H'_{ij}=H'_{ji}$, but the entries of H' are complex. Due to the simple structure of H' the matrix vector multiplication $\sum_j H'_{ij}\psi_j$ can be performed extremely fast on a vector computer. For this reason any diagonalization pro-

cedure that is iterative in the sense that it only uses matrix-vector multiplications to solve the eigenvalue problem would be very convenient. One such choice is the Lanczos procedure.[32–35] This is certainly a good choice for the calculation of the bound-state problem Eq. (12) since it is known to converge most speedily for the extreme eigenvalues. For the coupled-channel problem Eq. (10), it cannot be applied as it stands.

We have chosen to use a slightly different version of the algorithm, using our knowledge of the bound-state reference problem. We first calculate the eigenvector corresponding to the lowest eigenvalue of the zeroth-order Hamiltonian $\frac{1}{2}p^2+V_0(r)$. This can be done using the ordinary Lanczos procedure (for complex symmetric matrices, since we scale the bound-state problem as well). If we expand this eigenvector with zeros for the channels either above or below this single channel, we can consider this as an estimate for an eigenvector of the full Hamiltonian (we know this is exactly true for $\omega\to\infty$). If we take this vector as a starting value in the Lanczos iteration and use a sufficient number of iterations, we expect rapid convergence to the eigenvalue of the full matrix closest to the bound-state eigenvalue.

VI. RETURN TO THE LAB FRAME

The results obtained by solving the present coupled-channel problem are all given in the accelerated frame. If we return to the lab frame we can easily show that the fact that the wave function in the Kramers frame looks like

$$\chi(\mathbf{r},t)\approx\sum_{m=N_1}^{N_2}\psi_m(\mathbf{r})\exp[i(E_0-m\omega)t] \tag{38}$$

implies

$$\begin{aligned}\phi(\mathbf{r},t)&\approx\sum_{m=N_1}^{N_2}\psi_m(\mathbf{r}-\boldsymbol{\alpha}(t))\exp[i(E_0-m\omega)t]\\&=\sum_{k=-\infty}^{\infty}\sum_{m=N_1}^{N_2}\psi_{mk}(\mathbf{r})\exp\{i[E_0-(m+k)\omega]t\}\ ,\end{aligned} \tag{39}$$

where ϕ denotes the wave function in the lab frame and ψ_{mn} the nth Fourier component of $\psi_m(\mathbf{r}-\boldsymbol{\alpha}(t))$. Thus the Floquet decomposition of ϕ is approximately

$$\begin{aligned}\phi(\mathbf{r},t)&=\sum_n\phi_n(\mathbf{r})\exp[i(E_0=n\omega)t]\\&\approx\sum_{n=-\infty}^{\infty}\left[\sum_{m=N_1}^{N_2}\psi_{m(n-m)}(\mathbf{r})\right]\exp[i(E_0-n\omega)t]\ .\end{aligned} \tag{40}$$

This last equation can be used to demonstrate several things. First of all, it follows that the Floquet energies calculated by making a Floquet decomposition in the lab frame (as in Refs. 5–8) are identical to the ones obtained in the present approach. Second, it can be seen that, if a small number of channels suffices to describe the wave function in the Kramers frame of reference, this does not at all have to be the case in the lab frame; it depends on the behavior of the Fourier components of ψ_m.

Let us make one final remark about gauge invariance in this place. The Schrödinger equation in a purely electric field, Eq. (1), can be transformed from a form containing a $\mathbf{p}\cdot\mathbf{A}$ coupling term to a form containing a $\mathbf{E}\cdot\mathbf{r}$ coupling term. This is an electromagnetic gauge transformation, and thus all operators involving only the coordinates of the electrons and their expectation values remain unchanged.

Due to its similarity to this gauge transformation, the Kramers form of the Hamiltonian is also called the "acceleration gauge." Note that the Kramers transform Eq. (5) is not an electromagnetic gauge transformation (that is the reason why the term "acceleration gauge" is not used in this paper). The transformation (5) intertwines coordinates and electromagnetic fields, so that there are no simple invariant operators.

VII. RESULTS

A. Qualitative behavior

We implemented the finite difference equations in a computer code. The program was tested on the eigenvalue problem for H_2^+, with satisfactory results. We checked the bound-state energies of V_0 against the results listed in Ref. 15, which were calculated using a Gaussian basis. For the typical examples discussed below, where we do not use a large number of grid points, the accuracy of the ground-state energy is in the order of a few percent, though we can reach large accuracy.

Before going to the complete problem for H it is useful to study the effect of the scaling transformation Eq. (23) on $\frac{1}{2}\mathbf{p}^2$. The number of grid points is chosen so that one can expect reasonable accuracy of the results. We used 12 grid points in the ν coordinate and 36 in the μ coordinate. The upper bound on the μ coordinate is chosen 4.2, the scaling angle $\theta=0.35$ rad, a value that is typical for most scaling calculations [note again that *only* the states with σ symmetry ($m=0$) are studied here].

As one can see in Fig. 3 the results fall almost perfectly on a straight line for small energies—small wavelengths that do not feel the boundary—and show some spread at larger energies. As can be seen most clearly in the inset (low-energy spectrum), the angle of descent into the complex plane is exactly 0.7 rad, as was expected. This numerical check indicates that our assumption that the resulting spectral deformation is identical to that of ordinary complex scaling may be correct.

It is important to note here that the scatter of energies for higher real parts is typical for the type of solution method we use; in usual basis set methods one would not find this. The effects on energies and widths are small, as

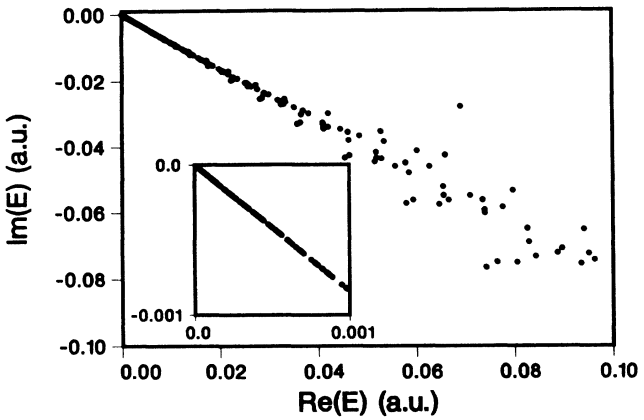

FIG. 3. Spectrum of $\frac{1}{2}\mathbf{p}^2$ for $C=4.2$, $n_\nu=12$, and $n_\mu=36$. The scaling angle θ is 0.35 rad. The inset shows the small energy points.

can be checked by increasing the grid size and the number of grid points.

In Fig. 4 the spectrum of the Hamiltonian $\frac{1}{2}\mathbf{p}^2+V_0(\alpha_0,\mathbf{r})$ is displayed for the same parameters as above. We use $\alpha_0=20$ as being a case that has all characteristics of the problem (see Ref. 15). In the figure one can see several interesting effects, which are enlarged in the insets for more clarity. In the inset on the left one sees that two continua with different threshold descent into the complex plane. This can be understood by considering the fact that V_0 is symmetric under a parity transformation, so that the eigenstates of *gerade* and *ungerade* symmetry (i.e., of even and odd parity) do not mix. Since a finite difference approximation is used, a (small) error is made in the calculation of all our integrals, of the same order of magnitude but not necessarily of the same size. Therefore the thresholds for the two continua (σ_g and σ_u) need not coincide, as one sees here.

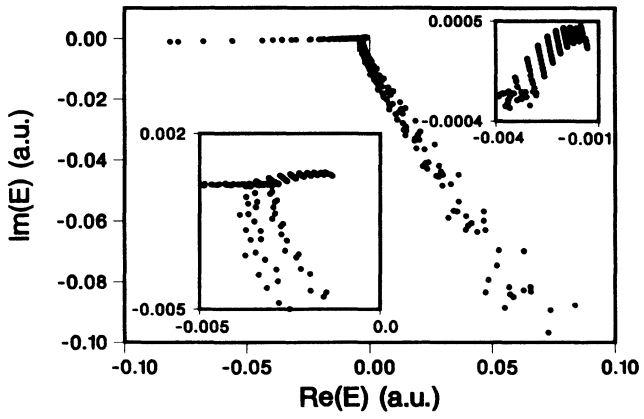

FIG. 4. Spectrum of $\frac{1}{2}\mathbf{p}^2+V_0(\alpha_0,\mathbf{r})$ at $\alpha_0=20$. The parameters are the same as in Fig. 3. The inset on the left shows an enlarged version of the threshold behavior, the one on the right shows the "unphysical" states above threshold.

This is very different from what happens in the usual basis set approach, but need not concern us very much since the difference between the thresholds, as well as their value, goes to zero as the discretization steps h_μ and h_ν go to zero.

This is not true for the feature shown in the inset on the right where one sees that there is a large number of states at positive imaginary energy, above threshold but below $\mathrm{Re}(E)=0$. This phenomenon is related to the shift of the threshold to a value below $E=0$; both phenomena are strongly influenced by the size of the cutoff parameter C_ν. The states at positive imaginary energy correspond to high-lying Rydberg states of the potential. Since a cutoff was applied in the radial direction, these states cannot be described accurately. The coupling to bound states of lower energy is not affected by this cutoff, so that after complex scaling, which causes a coupling of all the real-energy states found before scaling, the decay to the Rydberg states is described well. The decay from these Rydberg states to the continuum is dominated by the part that is outside the integration range. For this reason one finds a positive imaginary part. The shift of the threshold to values below zero is caused by the fact that the orthogonalization to a full Rydberg series is needed to get the low-energy continuum wave functions at the right place. This accords to the well-known fact that the distortion of continuum states in a Coulomb potential is strongest near threshold. The reader should note that this problem is not going to influence the results for the low-energy bound states. This is again a difference with a basis set method, where an incomplete basis for the higher excited states (a translation of what happens here) does not manifest itself with this signature.

Now consider two typical cases for the coupled-channel problem Eq. (11). Somewhat smaller values of n_ν and n_μ, 10 and 12, respectively, are taken in order to keep our matrices relatively small.

First the case of small ω is considered, $\omega=0.1$ a.u.$=2.72$ eV, so that $\lambda=456$ nm, which is in the visible spectrum. The intensity corresponding to $\alpha_0=20$ is $I=7\times10^{15}$ W/cm^2, which is large but not extremely high. These cases are more similar to those studied by Tang and Shakeshaft[8] and by Chu and Cooper.[6] The value of α_0 is larger than what these authors use, however (about 1). In these calculations one mostly finds small shifts to more negative values of binding energy. In Fig. 5 one can see a pole pair at the low energy of the spectrum that I think is caused by the increase in ionization potential. One should note that it is hard to decide on the position of a resonance since all calculations give a result modulo ω. Another feature that can be seen in Fig. 5 and more clearly in Fig. 6 is that there is no convergence. One would expect that the spectrum would not change any longer if enough channels were taken into account. This appears not to be the case, which is not surprising since this is not the range where the high-frequency and high-intensity approximations make sense; one would certainly need a much larger number of channels.

A case where one expects the theory to apply when taking into account only a few channels is $\omega=0.5$ a.u.$=13.5$ eV, $\lambda=91$ nm. Keep α_0 at the value 20, which

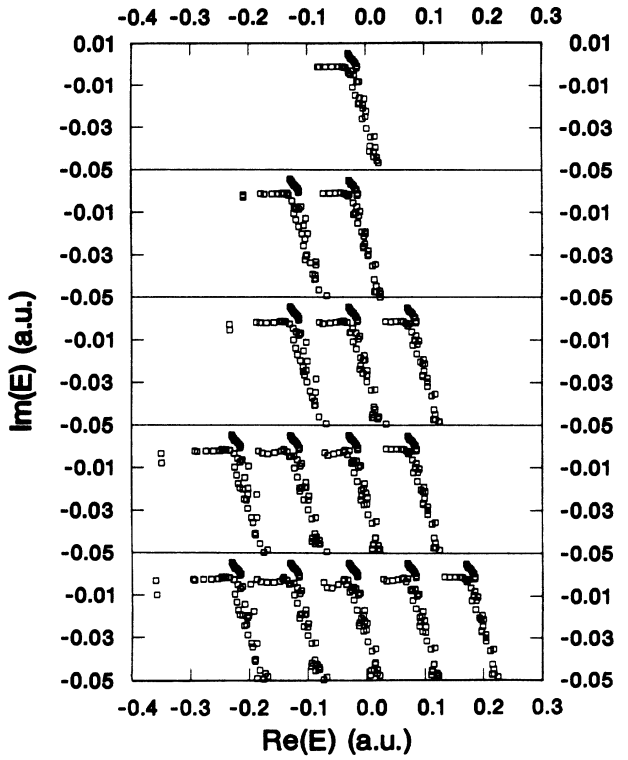

FIG. 5. Spectra for the channel-coupling Hamiltonian Eq. (11). The finite-difference parameters are $C=1.4$, $n_v=10$ and $n_\mu=12$. The scaling angle is 0.35 rad and $\omega=0.1$ a.u. Results for one to five channels are shown.

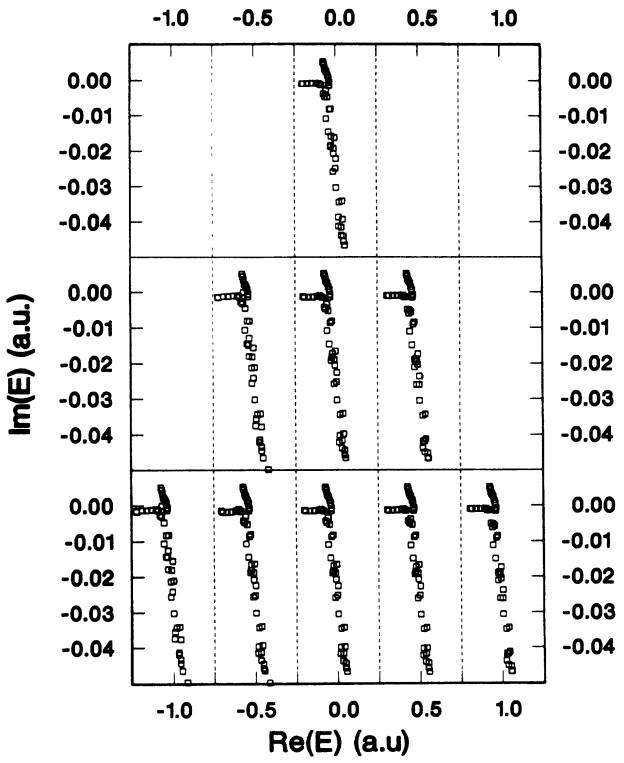

FIG. 7. Spectra for the channel coupling Hamiltonian Eq. (11). The finite-difference parameters are $C=1.4$, $n_v=10$, and $n_\mu=12$. The scaling angle is 0.35 rad and $\omega=0.5$ a.u. Results for one, three, and five channels are shown. The dashed lines indicate a discontinuity in the energy scale; at each line a step of 0.3 a.u. is taken.

means $I=1.75\times10^{17}$ W/cm^2. As one can see in Figs. 7 and 8 convergence is present in this case; there is hardly any difference between the case with three and five channels. The strange poles found in Fig. 5 are also not present. Identifying the eigenvalue that is lowest in each channel with the ground state (as can be done for $\omega=\infty$), one sees that the shift of the ground state is large and the width small.

B. Quantitative results

In order to study the behavior of the width as ω increases, we have studied the ground-state pole for $\omega=0.5$, 0.75, 1, 2, 4, and ∞ (the single-channel case). Only five channels were used (justified by the previous calculation) and more grid points ($N_v=40$ and $N_\mu=172$). One

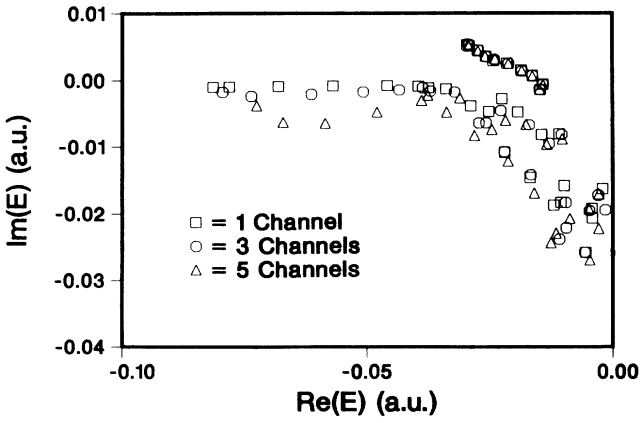

FIG. 6. Comparison of the energies of the states in the energy range $-0.1<\mathrm{Re}(E)<0$, for the states of Fig. 5, for one, three, and five channels.

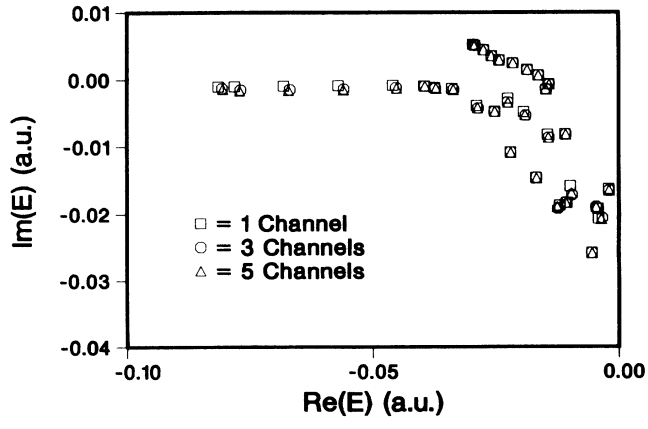

FIG. 8. Comparison of the energies of the states in the energy range $-0.1<\mathrm{Re}(E)<0$, for the states of Fig. 7, for one, three, and five channels.

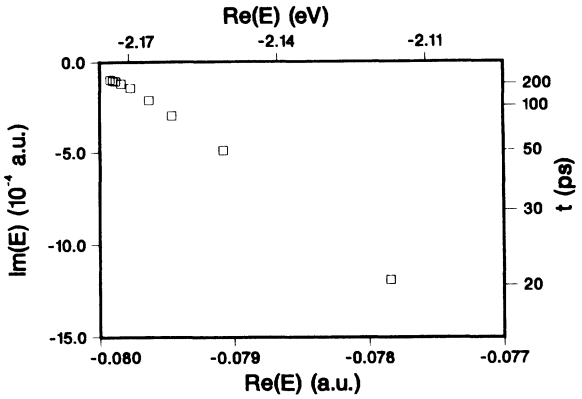

FIG. 9. Complex energy position for the ground state for $\alpha_0=20$ and (from right to left) ω is 0.5, 1, 1.5, 2, 3, 4, 6, 8, and ∞. The axes to the left and under the figure give the scale in a.u. The axis above the figure gives the energy scale in eV, the one to the right the half-life τ in picoseconds.

can easily see from Fig. 9 that high accuracy is necessary for calculations of the widths since these are very small in general. The imaginary part of the state at infinite frequency shows the limited accuracy of the present calculation; this state is a bound state and should have imaginary part zero. Clearly, we indeed find that the results converge as ω increases. This gives once more a confirmation of the consistency of the high-frequency and high-intensity limit.

It remains to compare our method with the "standard" low-frequency theory. We have taken one specific example from the papers by Shakeshaft and Tang[8] and Chu and Cooper.[6] This is the energy and width of the ground state for $\alpha_0=0.3$, $\omega=0.6$. (All the other parameters used in these papers correspond either to smaller ω or smaller α_0.) A calculation was performed with $N_\mu=15$, $N_\nu=5$ and 7 channels (the small value of N_ν can be justified by the expectation that for such a small value of α_0 the wave function is still almost spherical). The value for the ground-state energy in this field was $E_0=-0.4931-i0.0081$, and should be compared to $E_0=-0.4987-i0.0071$ from Refs. 6 and 8, so within the (limited) accuracy of the present calculation the results agree. We tried to increase the accuracy of the present calculation, but were limited by the fact that if α_0 becomes small, the two-center coordinates used here are not such a good choice and lead to numerical instabilities. Part of these appear in the solution of the Lanczos problem for the scaled bound-state equation, and could presumably be surmounted by transferring our program to a larger computer system, since we are limited by the amount of computer memory available. Still it shows that the region of small α_0 is not easily accessible using our present approach.

VIII. CONCLUDING REMARKS

The results given in this paper show that in high-intensity and high-frequency laser fields a calculation can be performed of the energy and of the lifetime of an atom in the Kramers gauge. Especially for cases where the frequency ω is a few times $E_0(\alpha_0)$, the convergence of our coupled-channel method is quite fast. Since $E_0(\alpha_0)$ is a decreasing function of α_0 (see Ref. 15), the method can be applied to optical frequencies when $\alpha_0\approx 10$.

The scaling of the ξ coordinate we have introduced in order to be able to perform the calculation can be used in *any* system where the potential has singularities on a line. It may therefore be used in the description of single-photon ionization of diatomic molecules or of electron scattering from diatomic molecules.

The reader should not be misguided by some of the apparent complications of the finite-difference method. The method leads to sparse matrix problems, and for that reason is very efficient, even for matrix dimensions that are huge (say, a million by a million). We never have to store the matrix itself, since it is very easy to write a compact and efficient routine that performs the matrix-vector multiplications needed in the Lanczos procedure. As such, the method shows promise for the treatment of atomic behavior in high-frequency laser fields.

The applicability of the present method is limited by the fact that high-intensity laser are always pulsed. So, for low frequencies, even when the high-frequency condition holds for the peak intensity, it does not hold for the flanks of the pulse, where intensities are much lower. In order to be able to perform experiments with lasers of optical frequencies, one might think of a two-laser experiment. Here one pulsed laser would pump a transition from the ground state to an excited state. A second continuous wave laser would be used to provide a beam that is high-frequency high-intensity for the excited state, but is chosen to be so weak that it does not perturb the ground state. Such experiments (and some refinements) would be very useful to establish the merits of the present theory.

ACKNOWLEDGMENTS

The author would like to thank Professor D. Kolb and Dr. D. Heinemann for their hospitality and useful discussions about finite-element and finite-difference methods. He would also like to thank Professor M. Gavrila, Dr. H. Muller, and Dr. M. Pont for valuable discussions about the physics of multiphoton ionization. This work was supported by the foundation FOM, which is a division of the Netherlands Organization for the Advancement of Research (NWO).

APPENDIX: FINITE DIFFERENCES

We will discuss here the scaled version of Eq. (24), approximated on a grid through a finite-difference approach. It is easy to see that the quantum number m is conserved, so that we only need to consider ∂_ϕ as constant. For convenience we take $m=0$, but similar results can be obtained for other values of m.

So we want to solve the equation

$$\frac{\delta}{\delta\phi}\int \phi(H-E)\phi\, d^3r \ . \tag{A1}$$

Consider the confocal elliptical coordinates (ξ,η,ϕ). We choose the polarization vector $\mathbf{e}$ along the z axis,

$$\begin{aligned}&\xi=(r_+ + r_-)/2\alpha_0 ,\\ &\eta=(r_+ - r_-)/2\alpha_0 ,\\ &\mathbf{r}_\pm=\mathbf{r}\pm\alpha_0\mathbf{e} .\end{aligned} \tag{A2}$$

Making one more change of coordinates,

$$\mu=\cosh\xi , \tag{A3}$$

$$\nu=\cos\eta , \tag{A4}$$

where $0<\nu<\pi$, $0<\mu<\infty$, one can readily derive the form of H_θ

$$H_\theta=\left[-\frac{1}{2\alpha_0^2}\frac{1}{e^{2i\theta}\sinh^2\mu+\sin^2\nu}\left[\frac{(1+e^{2i\theta}\sinh^2\mu)^{1/2}}{e^{i\theta}\cosh\mu}\frac{1}{\sinh\mu}\partial_\mu\sinh_\mu\frac{(1+e^{2i\theta}\sinh^2\mu)^{1/2}}{e^{i\theta}\cosh\mu}\partial_\mu + \frac{1}{\sin\nu}\partial_\nu\sin\nu\partial_\nu\right]\right]+V(\xi'(\mu),\eta(\nu)) . \tag{A5}$$

The boundary condition at the limits of the coordinates are

$$\begin{aligned}&\partial_\mu\phi|_{\nu=0}=0 ,\\ &\partial_\mu\phi|_{\nu=\pi}=0 ,\\ &\partial_\nu\phi|_{\mu=0}=0 .\end{aligned} \tag{A6}$$

Performing one partial integration, one can now easily derive a useful form for the action integral that contains at most first derivatives

$$I_\theta=\int d\nu\,d\mu\left\{\frac{1}{2\alpha_0^2}\left[\sinh\mu\sin\nu\frac{(1+e^{2i\theta}\sinh^2\mu)^{1/2}}{e^{i\theta}\cosh\mu}\partial_\mu\left[\frac{\sinh^2\mu+\sin^2\nu}{e^{2i\theta}\sinh^2\mu+\sin^2\nu}\frac{(1+e^{2i\theta}\sinh^2\mu)^{1/2}}{e^{i\theta}\cosh\mu}\phi\right]\partial_\mu\phi + \sinh\mu\sin\nu\partial_\nu\left[\frac{\sinh^2\mu+\sin^2\nu}{e^{2i\theta}\sinh^2\mu+\sin^2\nu}\phi\right]\partial_\nu\phi\right]+(\sinh^2\mu+\sin^2\nu)\sinh\mu\sin\nu(V(\xi'(\mu),\eta(\nu))-E)\phi^2\right\} \tag{A7}$$

Making use of Eq. (A6), we see that for a calculation of the derivatives through finite differences it is not very useful to integrate over the first interval near the border (this gives zero to the same order as the accuracy of the finite differences), where these are zero. In a one-dimensional example it can clearly be seen that a choice of function values at $(n+\frac{1}{2})h$, where h is the discretization step, is very convenient. The derivatives at the points nh can be approximated through finite differences as $f'(nh)\approx[f((n-\frac{1}{2})h)-f((n+\frac{1}{2})h)]/h$, the integrals over derivatives can be evaluated through the iterated midpoint rule [from $(n-\frac{1}{2})h$ to $(n+\frac{1}{2})h$], and the integrals over function values through the midpoint rule from nh to $(n+1)/h$. The accuracy thus obtained is $O(h^2)$. The final expression is

$$I(\boldsymbol{\phi})=\frac{1}{2\alpha_0^2}\left[\frac{1}{h_\mu^2}\sum_{m=0}^{N_\mu-2}\sum_{n=0}^{N_\nu-1}W^1_{m+1/2,n}(\phi_{nm}-\phi_{m+1,n})(V^1_{mn}\phi_{mn}-V^1_{m+1,n}\phi_{m+1,n}) + \frac{1}{h_\nu^2}\sum_{m=0}^{N_\mu-1}\sum_{n=0}^{N_\nu-2}W^2_{m,n+1/2}(\phi_{mn}-\phi_{m,n+1})(V^2_{mn}\phi_{mn}-V^2_{m,n+1}\phi_{m,n+1})\right] + \sum_{m=0}^{N_\mu-1}\sum_{n=0}^{N_\nu-1}[(V_{mn}-E)g_{mn}\phi^2_{mn}] , \tag{A8}$$

where the indices mn denote evaluation in $\mu=(m+\frac{1}{2})h_\mu$, $\nu=(n+\frac{1}{2})h_\nu$, and the function W and V are

$$\begin{aligned}&W^1=\sinh\mu\sin\nu\frac{(1+e^{2i\theta}\sinh^2\mu)^{1/2}}{e^{i\theta}\cosh\mu} ,\\ &V^1=\frac{\sinh^2\mu+\sin^2\nu}{e^{2i\theta}\sinh^2\mu+\sin^2\nu}\frac{(1+e^{2i\theta}\sinh^2\mu)^{1/2}}{e^{i\theta}\cosh\mu} ,\\ &W^2=\sinh\mu\sin\nu ,\\ &V^2=\frac{\sinh^2\mu+\sin^2\nu}{e^{2i\theta}\sinh^2\mu+\sin^2\nu} ,\\ &g_{mn}=(\sinh^2\mu+\sin^2\nu)\sinh\mu\sin\nu .\end{aligned} \tag{A9}$$

These last equations were used in the computer code.

The formulas discussed in this section are only valid for the operator H_0. The extension with the off-diagonal potentials is straightforward and is easily derived in a similar fashion as the integrations for V_0, the potential part of H_0.

---

*Present address: Department of Physics, University of Pennsylvania, Philadelphia, PA 19104-6396.

[1]P. Kruit, J. Kimman, H. G. Muller, and M. J. van der Wiel, Phys. Rev. A **28**, 248 (1983).

[2]P. Francken and Joachain, Phys. Rev. A **36**, 1663 (1987).

[3]K. C. Kulander, Phys. Rev. A **36**, 2726 (1987).

[4]*Multiphoton Ionization of Atoms,* edited by S. L. Chin and P. Lambropoulos (Academic, New York, 1984).

[5]A. Maquet, S.-I. Chu, and W. P. Reinhardt, Phys. Rev. A **27**, 2946 (1983).

[6]S.-I. Chu and J. Cooper, Phys. Rev. A **32**, 2769 (1985).

[7]X. Tang and R. Shakeshaft, Z. Phys. D **5**, 27 (1987).

[8]R. Shakeshaft and X. Tang, Phys. Rev. A **36**, 3193 (1987).

[9]H. A. Kramers, *Collected Scientific Papers* (North-Holland, Amsterdam, 1956), p. 866.

[10]W. C. Henneberger, Phys. Rev. Lett. **21**, 838 (1968).

[11]F. H. M. Faisal, J. Phys. B **6**, L89 (1973).

[12]J. I. Gersten and M. H. Mittleman, J. Phys. B **9**, 2561 (1976).

[13]M. Gavrila and J. Z. Kaminski, Phys. Rev. Lett. **52**, 614 (1984).

[14]M. Gavrila, in *Fundamentals of Laser Interactions,* edited by F. Ehlotzky (Springer, Berlin, 1986).

[15]M. Pont, N. R. Walet, M. Gavrila, and C. W. McCurdy, Phys. Rev. Lett. **61**, 939 (1988); Phys. Rev. A **41**, 477 (1990).

[16]J. N., Bardsley and M. J. Comella, Phys. Rev. A **39**, 2252 (1989).

[17]M. Floquet, Ann. Ec. Norm. Sup. (2) **XII**, 47 (1883).

[18]A. Tip, J. Phys. A **16**, 3327 (1987).

[19]K. Yajima, J. Math. Soc. **29**, 729 (1977); Commun. Math. Phys. **81**, 331 (1982).

[20]C. K. Choi, W. C. Henneberger, and F. C. Sanders, Phys. Rev. A **9**, 1895 (1974).

[21]B. R. Juncker, Adv. At. Mol. Phys. **18**, 207 (1982).

[22]W. P. Reinhardt, Annu. Rev. Phys. Chem. **33**, 223 (1982).

[23]B. Simon, Int. J. Quantum Chem. **14**, 529 (1978).

[24]A. J. F. Siegert, Phys. Rev. **56**, 750 (1939).

[25]*Handbook of Mathematical Functions,* edited by M. Abramowitz and I. A. Stegun (Dover, New York, 1972), p. 752.

[26]Assuming that the difference between the result of the present transformation and ordinary complex scaling is relatively compact with respect to $e^{2i\theta}p^2$, the continuous spectrum behaves as for ordinary scaling, i.e., it descends under an angle 2θ into the complex energy plane. See T. Kato, *Perturbation Theory for Linear Operators* (Springer, Berlin, 1966).

[27]E. Brändas and P. Froelich, Phys. Rev. A **16**, 2207 (1977).

[28]L. Laaksonen, D. Sundholm, and P. Pyykkö, Comput. Phys. Rep. **4**, 313 (1986); Int. J. Quantum Chem. **27**, 601 (1985).

[29]W. Schulze and D. Kolb, Chem. Phys. Lett. **122**, 271 (1985); D. Heinemann, D. Kolb, and B. Fricke, *ibid.* **137**, 180 (1987).

[30]M. Duff, H. Rabitz, A. Askar, A. Cakmak, and M. Ablowitz, J. Chem. Phys. **72**, 1543 (1980).

[31]W. K. Ford and F. S. Levin, Phys. Rev. A **29**, 43 (1984).

[32]C. Lanczos, J. Res. Nat. Bur. Stand. Sect. B **45**, 255 (1950).

[33]C. C. Paige, J. Inst. Math. Appl. **10**, 373 (1972).

[34]J. M. van Kats and H. A. van der Vorst, University of Utrecht, Academisch Computer Centrum Report Nos. TR-3, 1976 and TR-7, 1977 (unpublished).

[35]J. K. Cullum and R. A. Willoughby, *Lanczos Algorithms for Large Symmetric Eigenvalue Computations* (Birkhäuser, Boston, 1985), Vols. I and II.